All-fiber devices based on photonic crystal fibers with integrated electrodes

Giancarlo Chesini,[1] Cristiano M.B. Cordeiro,[1,*] Christiano J.S. de Matos,[2] Michael Fokine,[3] Isabel C.S. Carvalho,[4] and J. C. Knight[5]

[1]*Instituto de Física "Gleb Wataghin", Universidade Estadual de Campinas – UNICAMP, Campinas, SP, Brazil*
[2]*Grupo de Fotônica, Universidade Presbiteriana Mackenzie, SP, Brazil*
[3]*Department of Applied Physics – Laser Physics, KTH, AlbaNova University Center, Sweden*
[4] *Departamento de Física, PUC-Rio, Rio de Janeiro, Brazil*
[5]*Department of Physics, University of Bath, Claverton Down, Bath, BA2 7AY, United Kingdom*
[*] *cmbc@ifi.unicamp.br*

Abstract: A special kind of microstructured optical fiber is proposed and fabricated in which, in addition to the holey region (solid core and silica-air cladding), two large holes exist for electrode insertion. Either Bi-Sn or Au-Sn alloys were selectively inserted into the large holes forming two parallel, continuous and homogeneous internal electrodes. We demonstrate the production of a monolithic device and its use to externally control some of the guidance properties (e.g. polarization) of the fiber.

©2009 Optical Society of America

OCIS codes: (060.2310) Fiber optics; (230.3990) Microstructure devices; (999.999) Photonic crystal fibers.

References and links

1. P. Russell, "Photonic crystal fibers," Science **299**, 358-362 (2003).
2. J. C. Knight, "Photonic crystal fibres," Nature **424**, 847-851 (2003).
3. J. M. Fini, "Microstructure fibers for optical sensing in gases and liquids," Meas. Sci. Technol. **15**, 1120-1128 (2004).
4. C. M. B Cordeiro, M. A. R. Franco, G. Chesini, E. C. S. Barretto, R. Lwin, C. H. Brito Cruz, and M. C. J. Large, "Microstructured-core optical fibre for evanescent sensing applications," Opt. Express **14**, 13056-13066 (2006).
5. F. M. Cox, A. Argyros, and M. C. J. Large, "Liquid-filled hollow core microstructured polymer optical fiber," Opt. Express **14**, 4135-4140 (2006).
6. J. Jensen, P. Hoiby, G. Emiliyanov, O. Bang, L. H. Pedersen, and A. Bjarklev, "Selective detection of antibodies in microstructured polymer optical fibers," Opt. Express **13**, 5883-5889 (2005).
7. T. T. Larsen, A. Bjarklev, D. S. Hermann, and J. Broeng, "Optical devices based on liquid crystal photonic bandgap fibres," Opt. Express **11**, 2589-2596 (2003).
8. F. Du, Y. Lu, and S. Wu, "Electrically tunable liquid-crystal photonic crystal fiber," Appl. Phys. Lett. **85**, 2181-2183 (2004).
9. M. Fokine, L. E. Nilsson, A. Claesson, D. Berlemont, L. Kjellberg, L. Krummenacher, and W. Margulis, "Integrated fiber Mach-Zehnder interferometer for electro-optic switching," Opt. Lett. **27**, 1643-1645 (2002).
10. N. Myrén, M. Fokine, O. Tarasenko, L. E. Nilsson, H. Olsson, and W. Margulis, "In-fiber electrode lithography," J. Opt. Soc. Am. B **21**, 2085-2088 (2004).
11. K. Lee, P. Hu, J. L. Blows, D. Thorncraft, and J. Baxter, "A 200m optical fiber with integrated electrode and its poling," Opt. Lett. **29**, 2124-2126 (2004).
12. H. Knape and W. Margulis, "All-fiber polarization switch," Opt. Lett. **32**, 614-616 (2007).
13. Z. Yu, W. Margulis, O. Tarasenko, H. Knape, and P.-Y. Fonjallaz, "Nanosecond switching of fiber Bragg gratings," Opt. Express **15**, 14948-14953 (2007).
14. R. A. Myers, N. Mukherjee, and S. R. J. Brueck, "Large second-order nonlinearity in poled fused silica," Opt. Lett. **16**, 1732-1734 (1991).
15. P. G. Kazansky and P. St. J. Russel, "Thermally poled glass: frozen-in electric field or oriented dipoles?," Opt. Commun. **110**, 611-614 (1994).
16. T. Fujiwara, D. Wong, and S. Fleming, "Large electrooptic modulation in a thermally-poled germanosilicate fiber," IEEE Photon. Technol. Lett. **7**, 1177-1179 (1995).

#104614 - $15.00 USD Received 30 Nov 2008; revised 16 Jan 2009; accepted 17 Jan 2009; published 27 Jan 2009

17. D. Wong, W. Xu, S. Fleming, M. Janos, and K. M. Lo, "Frozen-in electrical field in thermally poled fibers," Opt. Fiber Technol. **5**, 235-241 (1999).
18. B. J. Eggleton, C. Kerbage, P. S. Westbrook, R. S. Windeler, and A. Hale, "Microstructured optical fiber devices," Opt. Express **9**, 698-713 (2001).
19. J. G. Hayashi, C. M. B Cordeiro, M. A. R. Franco, and F. Sircilli, "Numerical and Experimental Studies for a High Pressure Photonic Crystal Fiber Based Sensor," in 1st Workshop on Specialty Optical Fibers and Their Applications, AIP Conference Proceedings 1055, 133-136 (2008).
20. A. Claesson, S. Smuk, H. Arsalane, W.Margulis, T. Naterstad, E. Zimmer, and A. Malthe-Sorenssen, "Internal Electrode Fiber Polarization," in Optical Fiber Communication Conference, 2003 paper MF35.

1. Introduction

Photonic crystal fibers (PCF's) are optical fibers with periodically arranged microscopic air holes that run along the entire fiber length [1, 2]. In the case of solid core PCF's the microstructure reduces the effective cladding refractive index allowing guidance by total internal reflection (TIR) in an undoped core. For hollow core PCF's the guidance mechanism is due to a photonic band gap. The development of these special optical fibers opens new possibilities in areas such as nonlinear optics and sensing because they allow broad control of the fiber's optical parameters through the design of the structure's geometry. The fiber characteristics can also be further tailored using post-processing. One possibility is the insertion, within the microstructure, of a wide variety of materials, such as liquids and gases [3-5], biological specimens [6] and electrically/magnetically/thermally sensitive materials, which can then be placed close to or within the fiber core. In the latter case, a typical material used is liquid crystal (LC), in which the optical properties (and so the guidance properties of the waveguide) are tuned by heating [7] or by the application of an external electric field [8] to the LC-PCF system.

Fibers that can have their optical properties externally controlled will enable different types of active fiber devices. These devices allow one to exploit the inherent qualities of optical fibers, such as mass production, long light-matter interaction length, robustness and, especially, easy integration with optical fiber systems. The active control of the device characteristics as well as the device construction itself can be significantly improved by integrating an electrode (a metal wire or film) into the fiber. So far, several reports have demonstrated different techniques and approaches for introducing continuous electrodes into conventional fibers, typically with a germanium doped core and one or two large holes for the electrode(s) [9-13]. Devices as long as three meters were produced by silver film deposition onto the insides of the holes [10] and a 200-meter long optical fiber with an internal electrode was demonstrated using a procedure in which the wire was inserted into the fiber during the drawing process [11]. In most of these studies the primary objective was to use the internal electrodes for thermal poling of the fiber [14-17]. Recently, ohmic heating of the wire has also shown to be an effective means of controlling the optical properties of the fiber [13].

The all-fiber PCF-based active devices reported so far use a different approach, e.g., using a polymer with a highly temperature-dependent refractive index that enables the development of variable optical attenuators or tunable grating filters [18]. Our approach here was to develop a special microstructured fiber containing two holes for internal electrodes and applying an electric field between the electrodes, or passing a current through them. The fact that the PCF optical and mechanical properties can be widely custom designed is a potential advantage of these waveguides relative to conventional fibers with integrated electrodes.

Borosilicate fibers (Fig. 1(a)) and silica fibers (Fig. 1(b)) were manufactured and tested for this work. The silica fiber had an external diameter of approximately 170 μm. The microstructure consists of five rings of air holes with a diameter (*d)* of 1.5μm and a 2.5μm diameter solid core. The average pitch (Λ) is 2.2μm and the ratio d/Λ is 0.68. The two large holes have a width of approximately 25μm and approximately 13.5μm separates them from the edges of the core. For the silica fiber the birefringence induced by the large holes is estimated to be 4.1×10^{-5}. These PCFs, as standard fibers, guide light by total internal

#104614 - $15.00 USD Received 30 Nov 2008; revised 16 Jan 2009; accepted 17 Jan 2009; published 27 Jan 2009
(C) 2009 OSA

reflection in a high index region. As there is no chemical doping, guidance relies on the index difference between the solid core and the effective refractive index of the holey cladding.

The integration of the electrodes into the fiber was performed by melting and then pressurizing the alloy into the large holes [9], rather than inserting wires during fiber drawing process or manually inserting them into the final fiber [17]. The advantage of the filling procedure is that it provides continuous electrodes that completely fill the cross-section of the holes, maintaining a constant core-electrode distance along the fiber. In addition, the process allows one to have metal-free fiber tips, which is important when splicing such a structure with other types of fibers. It should be noted that the technique is not time consuming and easily performed. Fibers were filled with two different low melting point (T_m) alloys: Bi-Sn (T_m = 139°C) and Au-Sn (T_m ~ 300 °C). Fig. 1(b) shows the large holes of the silica fiber filled with metal which forms the internal electrodes. As can be observed, the filling process has no detrimental effect on the microstructure as it is done at a temperature much lower than the softening temperature of silica (~ 1600 °C). Fig. 1(c) presents a lateral view of the borosilicate fiber and shows the continuity of the electrodes, visible as bright parallel lines.

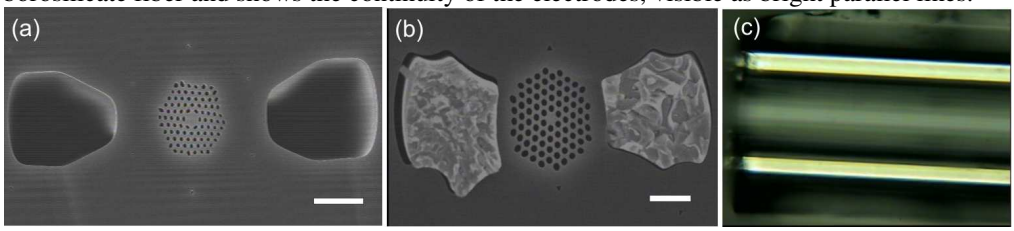

Fig. 1. (a) Cross-sectional view of the manufactured borosilicate PCF with two external holes. The white bar represents 10μm. (b) Scanning electron microscope image of the silica fiber with the two holes filled with metal. The white bar represents 10μm. (c) Lateral view of the borosilicate fiber with the internal electrodes (two parallel bright lines).

2. Experimental setup

To access the internal electrodes, the fiber was side polished until the previously inserted metal was exposed, which was followed by connecting the electrodes to an external circuit using a conductive silver epoxy. Two different configurations were studied, as shown in Figs. 2(a) and 2(b). In the first case we used the Bi-Sn alloy and externally connected the same electrode at two different points to enable a current to pass through the electrode. In the second case, Fig. 2(b), the two Au-Sn electrodes were externally connected to enable a high voltage to be applied between them. In the latter case it is important to have metal-free fiber tips, as in Fig. 2(c), in order to avoid electrical breakdown in the air between the electrodes.

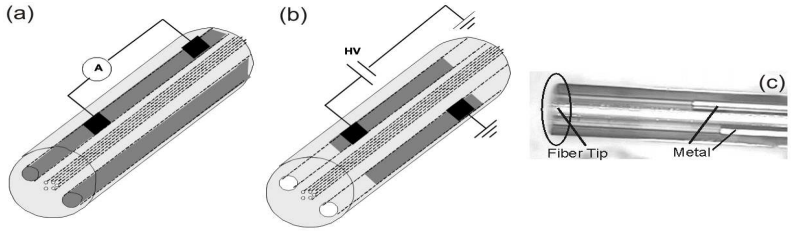

Fig. 2. (a) Bi-Sn-filled fiber with only one electrode exposed at two different places and connected to a current source. (b) Au-Sn-filled fiber with both electrodes exposed and connected to a high voltage (HV) source. (c) Lateral view of the fiber tip without metal.

To optically characterize the silica fiber with the setup of Fig. 2(a) (Bi-Sn alloy, current configuration) we used a linearly polarized He-Ne laser in a setup depicted in Fig. 3. The fiber was around 7 cm long.

#104614 - $15.00 USD Received 30 Nov 2008; revised 16 Jan 2009; accepted 17 Jan 2009; published 27 Jan 2009
(C) 2009 OSA

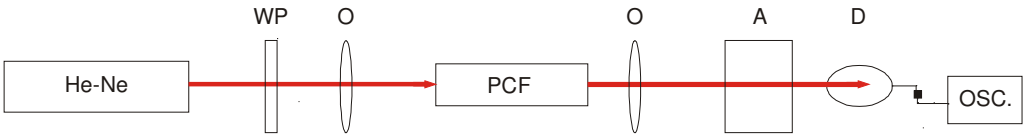

Fig. 3. Setup for optical characterization of the setup of Fig. 2(a) with a linearly polarized He-Ne laser. WP is a half-wave plate (for 633nm), O are objectives, A is a rotating polarizer and D a detector connected to an oscilloscope.

3. Results and discussion

The first step of the optical characterization consists of finding the fiber's polarization axes, in the absence of any applied current. To do that, the incoming polarization was controlled through a half-wave plate (WP) and the light leaving the fiber passed through a rotating analyzer (A) before reaching the detector (Fig. 3). For each WP angle we measured the maximum (I_{max}) and the minimum (I_{min}) intensities through the analyzer and computed the signal ellipticity, given by $(I_{min}/I_{max})^{1/2}$. This ellipticity is expected to vary periodically with the incoming polarization (period of 90°) and the measured data is shown in Fig. 4(a). The position corresponding to the first peak was chosen to be the reference angle (0°) from which the other angles were determined. The ellipticity minima (0°, 88°, 180°, 268° and 348°) are associated with light traveling along the birefringence axes and, thus, exiting the fiber with quasi-linear polarizations. The ellipticity maxima (48°, 128°, 220° and 304°) are seen to occur halfway between minima, which is a consequence of the relative delay induced for this particular fiber length. At 0° and 180° the input light is polarized along the axis that connects the electrodes, while at 88° and 268° it is perpendicular to this direction. It is important to note that the fiber length was not optimized for enhancing the visibility in Fig. 4(a), meaning that the ellipticity is not necessarily expected to reach 1 (circular polarization). On the other hand, the ellipticity also never reaches zero (linear polarization). A possible explanation to this feature is that the fiber presents some chirality (resulting from spinning during the drawing process), making the polarization eigenstates elliptical.

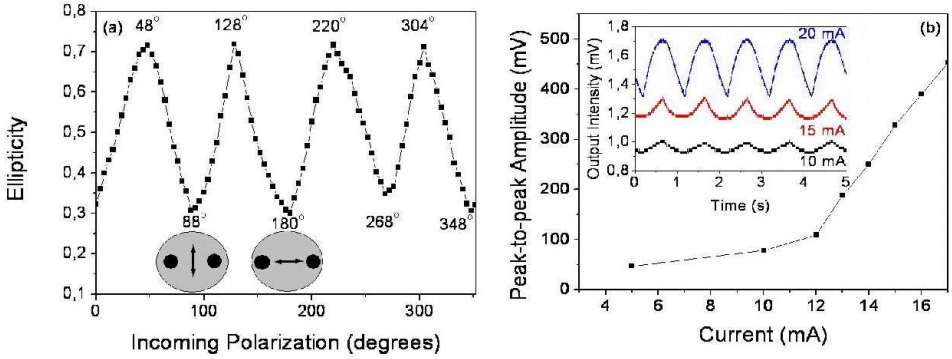

Fig. 4. (a) Polarization ellipticity of the light exiting the fiber filled with metal. (b) Intensity through the fixed analyzer as a function of the applied "square wave" electric current. The inset shows a real-time measurement of the output intensity through the analyzer for three different current amplitudes.

The next step was to apply an electric current to the fiber for 500ms and turning it off for another 500ms repeatedly, creating a "square-wave" current. During the time the electric current is on, the metal expands due to thermal effects and squeezes the microstructure inducing a birefringence change. Since we expect more sensitivity when input light is linearly polarized halfway between the birefringence axes, we fixed the incoming polarization at 48° (which maximized the ellipticity in Fig 4(a)). The analyzer was fixed in the position of maximum output intensity. The amplitude of the applied electric current (in the form of a square-wave signal) was varied from 5 to 20mA and the signal peak-to-peak amplitude (I_M-I_m)

#104614 - $15.00 USD Received 30 Nov 2008; revised 16 Jan 2009; accepted 17 Jan 2009; published 27 Jan 2009
(C) 2009 OSA

through the analyzer was measured. Fig. 4(b) shows the behavior of the signal amplitude in this situation. As it was expected, the amplitude increases with higher electric currents. It is clear that there is a threshold (around 12mA) from where the amplitude starts to grow at a higher rate. The inset of Fig. 4(b) shows the measurement of the output intensity versus time where it is possible to see the variation of the signal amplitude with the applied current.

Another important question is the mechanism by which the device operates. To investigate this, we applied a steady (dc) current for several seconds. The incoming polarization, as before, was set to give the most sensitive results ($\theta \sim 45°$). Again, the analyzer was fixed in the position of maximum transmitted intensity. Electric currents of 15 and 20mA were applied to the device while the output intensity was monitored, as shown in Fig. 5. When the electric current is switched on the birefringence of the fiber is modified and so is the state of polarization of the exiting beam. The rotation of polarization becomes an intensity variation due the presence of an analyzer after the fiber (Fig. 3). The number of maximum-minimum cycles the intensity undergoes depends on the applied current. The modeling of the detailed change of the cladding geometry and fiber birefringence with the electrode expansion is being carried out and will be published in a future work. It should be pointed out, however, that the presence of the cladding air holes not only allows a wider control of the fiber optical properties but also of its mechanical ones [19].

With this fiber, and at 15 mA, the system goes from maximum to minimum transmitted intensity while at 20 mA it goes from maximum to minimum and back to maximum. The same process occurs in the inverse order when the electric current is switched off and the polarization rotates back to its original state. The intensity peaks that appear just after the current being switched on are believed to be due the change of the polarization state from elliptical to linear along the analyzer axis before it evolves till a situation of orthogonal polarization with respect to the analyzer. It should be noted that these current values cannot be directly compared with those of Fig. 4(b) as in that case an oscillating current was used while here a continuous one was. The number of cycles observed in Fig. 5 for 20 mA suggests that the current-induced relative phase delay is close to π, from which the current-induced birefringence can be estimated to be $\sim 4.5\times10^{-6}$.

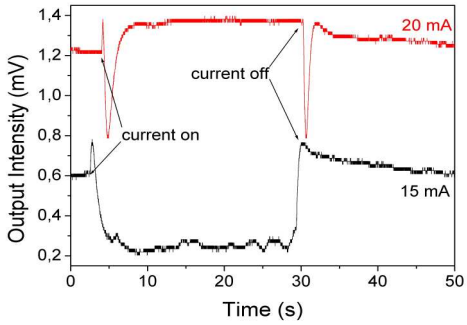

Fig. 5. Output intensity through the fixed analyzer as a function of time for two different steady electric currents (15 and 20mA). When the electric current is switched on the birefringence of the fiber is modified and the light state of polarization changes. The number of cycles the polarization undergoes depends on the value of the electric current.

The induced polarization rotation was also characterized as a function of the angle of the input polarization. The same "square-signal" electric current (fixed at 20mA) was applied to the device for three incoming linear polarizations: $\theta = 0°$ (aligned with one birefringence axis), $\theta = 24°$, and $\theta = 48°$ (polarization halfway between birefringence axes). For each polarization, the analyzer was fixed in the position of maximum output intensity. The results are shown in Fig. 6(a).

#104614 - $15.00 USD Received 30 Nov 2008; revised 16 Jan 2009; accepted 17 Jan 2009; published 27 Jan 2009
(C) 2009 OSA

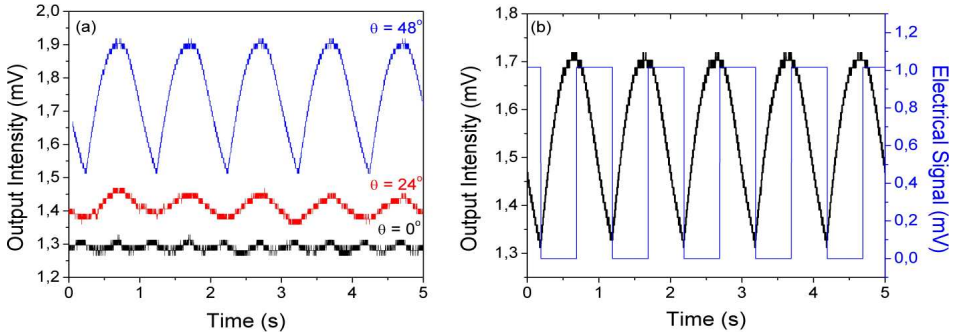

Fig. 6. (a) Output intensity through the fixed analyzer as a function of time for three different incoming polarizations. (b) Intensity through the fixed analyzer, for θ = 48°, as a function of time and the applied "square wave" electric current.

The curves were vertically shifted in order not to overlap. As expected, for θ = 0° (a birefringence axis) the electric current has little effect in the output intensity. In an ideal situation, one would expect to see no change in the output intensity due to external influences. As we move away from the birefringence axis (θ = 24° and θ = 48°), the effect caused by the metal expansion keeps growing until it reaches a maximum, when light travels with polarization halfway between the axes. Fig. 6(b) shows the output intensity through the fixed analyzer, when a 20-mA-amplitude square-wave current signal is applied and an input linear polarization with θ = 48° is used. It is possible to see that this 20mA electric current applied to our 7cm long device is sufficient to cause an appreciable change in the output intensity. Knowing the electrical resistance of the device (50 Ω) we can apply Ohm's Law to compute the voltage required to change the output intensity from a maximum to a minimum. We obtained a value of approximately one volt. Claesson et al. reported in standard-like fibers typical performance values of 2.5V in a 5cm device [20]. A direct comparison between both values cannot, however, be made due to the different signal repetition rates, duty cycles and fiber lengths (a linear dependence is expected between the device resistance and length, but a non-linear one is expected between current and optical response – see Fig. 4(b)). Microstructured fibers have, however, potential room for improving this figure by optimization of the cladding geometrical parameters and, consequently, of their mechanical properties, as previously suggested [19]. As the device operation relies on thermal effects, its response time can be rather slow, as it is in our case, where both the on/off states are related to heat dissipation. However, Knape and Margulis [12] demonstrated a nanosecond response time when using a nanosecond high-voltage pulse, indicating a way to improve this issue.

4. Conclusion

The possibility of having a microstructured optical fiber with integrated electrodes opens several interesting possibilities of playing with the insertion of electrically/temperature sensitive materials and the application of an external field for guidance control purposes. Here we developed a photonic crystal fiber with two large holes (externally to the microstructured cladding) to integrate electrodes, making a monolithic device based on the dynamic squeeze of the microstructure and its influence over its polarization properties. The fiber electro-optical characterization was carried out by first electrically connecting one of the electrodes and then applying an electric current to it while polarization rotation was monitored. We demonstrated that a 20mA electric current is sufficient to change the output intensity from a maximum to a minimum level. This represents 1 volt applied to a 7cm electrode.

Acknowledgments

The authors thank FAPESP, CNPq, CAPES and MackPesquisa for the financial support, M.A.R. Franco for modeling the fiber birefringence and Jose Aparecido for his technical help.

#104614 - $15.00 USD Received 30 Nov 2008; revised 16 Jan 2009; accepted 17 Jan 2009; published 27 Jan 2009
(C) 2009 OSA